

CERN LIBRARIES, GENEVA



CM-P00045063

CERN/SPSC/84-58
SPSC/M376 Add. 1
24 August 1984

M E M O R A N D U M

TO : The Members of the SPSC

FROM : M. Dris, N. Giannacopoulos, D. Lucas, E. Gazis and A. Maltezos
National Technical University, and N.R.C. Demokritos,
Athens, Greece.

E. Nappi and P. Spinelli,
Dipartimento di Fisica dell'Università di Bari, and INFN,
Sezione di Bari, Bari, Italy.

L. Camilleri, J. Kirkby(*), and K. Winter,
CERN, European Organization for Nuclear Research, Geneva,
Switzerland.

C.N. Booth and T.O. White,
Cavendish Laboratory, Cambridge University, Cambridge,
United Kingdom.

C. Joseph,
University of Lausanne, Lausanne, Switzerland.

A group from Junta de Energia Nuclear, Madrid, Spain.

J. Bunn, P. Freund, K.P. Pretzl, P. Seyboth and J. Seyerlein,
Max-Planck-Institut für Physik und Astrophysik, München,
München, West Germany.

R. Cool, P.T. Cox and R. Rusack,
Rockefeller University, New York, U.S.A.

M. Atkinson, D. Crenell and C. Fisher and P. Hughes,
Rutherford and Appleton Laboratory, Chilton,
Didcot, United Kingdom.

SUBJECT : Status Report of the Second Generation Calorimeter Detector for
the SppS Collider: ANAPHE(**) (Annihilation of Antiprotons and
Protons at High Energy).

(*) Contact person.

(**) Anaphe, meaning "revelation", is a small island in the Aegean Sea
which, according to mythology, was revealed one night to Jason and the
Argonauts by a blazing arrow from Apollo's bow.

1. INTRODUCTION

At the May 1984 meeting of the SPSC we presented the concept of a second generation calorimeter detector which is matched to the rich physics potential of the Sp \bar{p} S Collider with ACOL. We wish to present here a summary of the status of this detector in the light of the advice of the SPSC and of subsequent developments.

Our broad strategy for constructing the detector remains the same; we plan to build it in phases in order to ensure a startup which is competitive with the TeV I program. The first phase of the detector would be non-magnetic and later a superconducting solenoid would be added if funds became available. The essential points are as follows:

- The first phase of the detector has superior performance to both the upgraded UA1 and UA2 detectors, and can therefore already be justified under the assumption of no future upgrading.
- A well-understood upgrade program to better performance and higher energies and luminosities is built into the design of the detector. We see that upgrades have become a universal feature of large detectors due to the enormous investment of time and resources in the original equipment. Where we differ from the current detectors, however, is in our concept of a planned and therefore uncompromised upgrade.
- There is a serious lack at CERN of a detector which is optimized for hadron collider physics. Moreover, none of the new detectors under construction was designed after the UA1/UA2 results. There exists a strong hadron collider machine program with the ACOL upgrade and possibly the LEP Hadron Collider (LHC). Therefore, if a new calorimeter detector is initiated, we believe it must be designed with the possibility of a long period of operation and be readily upgradable to perform at higher energy and higher luminosity.

Our goal is to commence operation of the detector in 1989/1990. This date, which is later than our original aim of 1988 because of delays to our proposal, follows for two reasons:

- It is the earliest date by which the detector could be built, tested and installed.
- It is the startup date of a competitive 2nd round detector at the Fermilab TeV I Collider - the DØ detector.

In order to meet this goal of operation in 1989/1990, we have developed a strategy involving the minimum new construction for the first phase of the detector. Our aim is as follows:

- To construct a new central detector comprising of a uranium calorimeter with a compact inner detector: a scintillating optical fibre micro-tracker, transition radiation detector and Si pad (dE/dx) system.
- To construct an outer muon system comprising of magnetized steel absorber and large-area drift tubes or chambers.
- To utilize the UA2 upgrade end-caps (SPSC/P93 Add.2).
- To utilize the maximum possible UA2 infrastructure (cables, electronics, computers etc).

This approach will provide a detector with better performance than the upgraded UA1 and UA2 detectors at a fraction ($\sim 1/3$) of the cost of a LEP-scale detector. Nevertheless, this is an ambitious project and will require a substantially larger group of physicists than ourselves. We therefore propose a working group be initiated immediately to explore the physics potential of the ACOL and to design a second-round detector. This working group should be drawn from members of all UA collaborations, ourselves and other interested physicists. If this working group develops then the ideas presented here and in our previous memorandum (SPSC/M376) could become the starting point for discussions.

2. PHYSICS GOALS

2.1 General Comments

Our strong interest in the $S\bar{p}pS$ Collider is driven by an expectation of new and exciting physics. We believe the potential is strong for more dramatic physics discoveries to be made in this energy range, with the ten-fold luminosity increase of ACOL and with a new and optimized detector. The past discoveries of the $S\bar{p}pS$ Collider are spectacular - the W^\pm , Z^0 and perhaps t quark - and the future prospects are excellent. Hints of anomalous events have already been seen in UA1 and UA2 - involving jets and photons associated with large missing E_\perp and a di-jet mass bump. Further data taking will increase statistics but may not resolve the origin of these events. In many ways the situation is analogous to the proton decay program where each experiment has obtained a handful of strange events and what is needed is not only more data but also a new experiment with better performance.

Independently of the outcome of these anomalous events, the prospects for new physics in the ACOL energy range are excellent (see Tables 2 and 3 of SPSC/M376). A most important question to ask is: would the upgraded UA1 and UA2 fail to see a new physics signal where ANAPHE would not? We think the answer is yes, based on the discussion which follows in this section and the comparison of the performances of the detectors (section 4).

Our physics program involves studies of several broad topics at a new level of sensitivity:

- a) Lepton and multi-leptons study
 - top
 - mixing of heavy flavours
 - Drell Yan
 - new onia
 - flavour changing neutral currents
 - long-lived particles (secondary decay vertices)
 - new physics

- b) Missing energy study
 - ν
 - $\tilde{\nu}$
 - γ
 - heavy leptons
 - new physics

- c) Jet study
 - dimass spectrum ($W \rightarrow 2$ jets, new particles)
 - new physics

- d) Predicted new particles
 - Higgs
 - techniparticles eg $n_t \rightarrow t\bar{t}$
 - supersymmetric particles.

Among these topics we believe the most important are searches for new particles since their discovery exerts a major influence on our understanding of matter. In the framework of particles which are theoretically predicted, we single out the Higgs, techniparticles and supersymmetric particles as key goals for an ACOL detector. We will discuss in general terms the suitability of ANAPHE to detect these particles in the remainder of this section.

2.2 Higgs and Techniparticles

We group these particles together since both decay preferentially to the heaviest fermion pair allowed kinematically. Their production cross-sections are, however, quite different.

In the case of the Higgs, which has a large coupling to the W, the production occurs by:

- W decay: $\bar{p}p \rightarrow XW \rightarrow X H^0 f\bar{f}$
- Associated production: $\bar{p}p \rightarrow XWH^0$

The cross-section for these processes, relative to the total W rate is $\sim 5 \cdot 10^{-3}$ for $m_H = 10 \text{ GeV}/c^2$ falling to $\sim 10^{-4}$ for $m_H = 50 \text{ GeV}/c^2$. For an integrated luminosity of 10 pb^{-1} , corresponding to about three operational years with ACOL, we expect 64K produced W's of which 5.3K decay to $e\nu$. We see immediately that if a detector is restricted to the leptonic W decays there is no sensitivity to Higgs' above $\sim 20 \text{ GeV}/c^2$; in order to search in a higher mass range it is necessary to allow the real or virtual W to decay hadronically ($u\bar{d}$, $c\bar{s}$ or $t\bar{b}$).

A Higgs in the available mass range will decay almost entirely into $b\bar{b}$ quark pairs. We therefore see the best sensitivity to Higgs production requires:

- Detection of heavy flavour jets, especially b jets. These are produced both by the Higgs decay and in a large fraction of the W decays.
- Good calorimeter mass resolution.

The signatures of b jets are direct leptons, missing E_T and secondary decay vertices. Among these, it has already proved possible to pick out b jets using leptons in the clean environment of e^+e^- colliders. If b jets can be tagged with high efficiency at the SppS Collider then the QCD background can be strongly reduced relative to the Higgs signal and there will be an improved sensitivity to Higgs production. We will therefore discuss the detection of b jets in ANAPHE.

A lepton tag for b's can have a high efficiency; a primary lepton will be produced in $\sim 50\%$ of all Higgs decays. The lepton is however produced at low E_T . In the mass range of interest ($10 < m_{H^0} < 50 \text{ GeV}/c^2$) the b jets have $E_T \sim 10\text{-}35 \text{ GeV}$ and so the primary electrons have $E_T \sim 3\text{-}10 \text{ GeV}$. (We show in Fig. 1 a representative electron spectrum from QCD b jets in the range $20 < E_T^b < 35 \text{ GeV}$.) The fine transverse granularity of the electromagnetic calorimeter of ANAPHE is well-matched to the b jet particle density; 90% of these electrons are in singly-occupied cells. Finally we show (Fig. 2) the rapidity distribution of electrons produced in $W \rightarrow t\bar{b} + t\bar{c}e\nu$, which is also representative of electrons produced in Higgs decays. They are centrally produced and accepted with good efficiency in our central uranium calorimeter and transition radiation detectors.

Present analyses of UA1 and UA2 completely exclude b electrons by making minimum E_T cuts of 12 GeV (UA1) or 20-25 GeV (UA2), as well as severe isolation cuts. We illustrate our background situation in Fig. 3. We have chosen as a representative signal electrons produced in the decay $W \rightarrow t\bar{b}$. Despite our fine electromagnetic calorimeter granularity, the $\pi^\pm \gamma$ overlap rate is a factor $10^3\text{-}10^4$ higher than this signal. (This corresponds to the non-magnetic phase; there is an improvement by

about an order of magnitude after adding a solenoid and imposing an E/p match.) Rejection by $\sim 10^{-3}$ is probably available by a) requiring spatial coincidence of the incident track and the centroid of the transverse energy distribution in the electromagnetic calorimeter and b) requiring no penetration of energy through the back of the electromagnetic calorimeter. Both cuts require a fine grained calorimeter to avoid the influence of tracks in nearby cells. Finally, we can introduce an independent rejection factor of 10^{-2} using the transition radiation detectors. The outcome is a sensitivity to the b electrons over the full P_T range.

In the case of techniparticles, their small couplings to the gauge bosons imply a negligible production of P^0 or P^\pm with vector bosons. The most promising candidates are the colour octet pseudoscalars P_8 , which preferentially decay to $t\bar{t}$ (or $b\bar{b}$ at lower masses) and gg jets.

The overall conclusion is that the ability of ANAPHE to handle the low P_T electrons in b jets is a powerful tool in searches for new particles - especially in combination with the good jet mass resolution, missing E_T resolution and secondary vertex detection of the detector.

2.3 Supersymmetric Particles

The most favoured possibility is that the lightest sparticle is a stable photino $\tilde{\gamma}$. Consequently, the experimental signature of sparticle production and decay is $\tilde{X} \rightarrow X + \tilde{\gamma}$, $X = q, \ell, W$ etc. where the $\tilde{\gamma}$ escapes the detector analogously to a neutrino. This places a premium on missing E_T resolution, which we will now discuss.

We show in Fig. 4 several missing E_T distributions. The first point to note is that the comparison of curves c) and d) shows that only a modest deterioration in the quality of the missing E_T measurement will result by using the UA2 upgrade end caps with ANAPHE. The comparison between these uranium calorimeter measurements and a Pb/Fe calorimeter such as UA2 (curve e) shows a factor ~ 3 improvement in the level of missing E_T background due to instrumental resolution. The natural limit to detector performance is indicated by the rate of neutrino production (curve b). Most of this occurs through π/K decays in flight even though ANAPHE has a

short decay path of only ~ 80 cms. If we assume gaussian tails on the calorimeter energy measurements, we can extrapolate these data and estimate that \tilde{g} ($m = 70 \text{ GeV}/c^2$) pair production (curve a) can be observed above $E_T^{\text{missing}} \sim 40 \text{ GeV}$ with an efficiency of $\sim 20\%$.

However, dead regions (projective cracks) in a calorimeter create large deviations from gaussian tails. We have made a simple calculation to indicate the severity of this problem in current calorimeters and show the results in Fig. 5. As a model of a good calorimeter, where careful attention has been given to the reduction of dead regions, we chose the L3 hadron calorimeter which has azimuthally projective cracks totalling $\sim 5\% \times 2\pi$ radians. We have investigated two scenarios:

- Massive cracks (Fig. 5, curve d) which are filled with inert material. Incident particles are assumed to have a mean response of $1/2$ relative to nominal.
- Massless cracks (Fig. 5, curve e). Incident particles exit the calorimeter without depositing any energy.

We see even such an apparently small loss in hermeticity results in a dramatic increase in the tails of the missing E_T distribution. With these cracks a gluino search would be overwhelmed by the instrumental missing E_T background.

We stress that the hermeticity of a calorimeter is not something which can be achieved by a patch-up job on an existing hadron calorimeter with projective geometry (and therefore projective cracks). The successful construction of a hermetic calorimeter will require attention to details of the design which have only recently been appreciated e.g. in order to eliminate the influence of cracks it appears that they must be inclined by $\sim 10^\circ$ relative to the particle direction.

3. DETECTOR DEVELOPMENTS

3.1 Calorimeter

The calorimeter design is a uranium sampling device with scintillator readout using a double-shift into plastic fibres of narrow diameter (2 mm). We have successfully demonstrated that this readout technique gives excellent performance using phototubes (see Appendix A). Our next

measurements, which are taking place this month, will investigate the performance using Si photodiodes. These devices have many advantages over phototubes: better match to the small fibre size, cost, compactness, stability, uniformity of response and insensitivity to magnetic field. A further important technical question which we are investigating involves the radiation hardness and aging of the scintillator and wave-shifters in the calorimeter.

3.2 Micro-tracker

A key feature of the detector is a compact and precise central tracker made from scintillating optical fibres. This device allows the inner radius of the calorimeter to be reduced to only 60 cm, thereby minimizing the quantity of uranium required. (The central calorimeter involves 190 tons uranium and has a minimum depth of $6.3 \lambda_{\text{ABS}}$.) Within this radius there is space for a deep transition radiation detector (40 cm).

Our original memorandum considered the application of plastic scintillator fibres of diameter 100-300 μm . Since that time there have been new measurements by Ruchti et al (paper submitted to the XII Int. Conf. on High Energy Physics, Leipzig, 1984) using Ce_2O_3 glass fibres of diameter 10-25 μm which encourage us to keep open their possible application in ANAPHE. If successful, these very narrow fibres introduce superb performance e.g. momentum measurement error (with 1.5 T solenoid), $\sigma_p/p = 4 \cdot 10^{-4} p$ (GeV/c) $\oplus 4 \cdot 10^{-2}$, σ_{xy} per point = 10 μm , σ (impact parameter at origin) < 20 μm ($p > 20$ GeV/c) etc. (\oplus denotes addition in quadrature.) However, the understanding of both glass and plastic scintillating fibres has barely begun and there are many unanswered questions. We are therefore pursuing a vigorous R&D program to develop them into micro-trackers.

3.3 Muon System

The first phase of the detector will have a μ detection system comprising 1 m magnetized (2T) Fe covering the outer surface. Chambers measure the vector directions of tracks before and after this absorber. The muon system serves the following functions:

- Measurement of μ sign
- Measurement of μ momentum, $\sigma_p/p = 6 \cdot 10^{-4} p$ (GeV/c) $\oplus .19$

- Reduction of hadron punch-through background
- Improvement in the measurement of E_t^{missing} due to non-interacting neutral particles such as ν or $\tilde{\gamma}$. (In the case of a $\tilde{\gamma}$ search, events with a muon or electron will be vetoed.)

After a superconducting solenoid upgrade there would be three independent measurements of μ momentum:

- Inner micro-tracker, $\sigma_p/p = 4 \cdot 10^{-4} p$ (GeV/c) $\oplus 4 \cdot 10^{-2}$,
- Chambers placed at the outer surface of the solenoid, $\sigma_p/p = 2.5 \cdot 10^{-4} p$ (GeV/c) $\oplus 0.33$
- Magnet flux return, $\sigma_p/p = 10^{-3}$ (GeV/c) $\oplus .24$.

This will lead to an excellent rejection of hadron decay and punch-through background. In addition the matching between a μ identified in the outer system and its inner trajectory in the presence of jets will be substantially improved.

4. COMPARISON OF TECHNICAL PERFORMANCE WITH OTHER HADRON COLLIDER DETECTORS: UPGRADED UA1 and UA2, CDF, DØ

4.1 General Comments

The most important point to appreciate is that the experiences of UA1 and UA2 have transformed our view of the design features required in a hadron collider detector. Consequently, we can categorize such detectors as those designed before the first data from the Sp \bar{p} S Collider - UA1, UA2 and CDF - and those designed after - DØ and ANAPHE.

Both UA1 and UA2 have taught us that the crucial detector tool is calorimetry and, in particular, UA1 has demonstrated the unexpected power of a hermetic calorimeter to detect ν 's (or $\tilde{\gamma}$'s) down to very low values of E_T (~ 10 GeV). Each of the original detectors is seeking to make modifications which will correct its weaknesses, but only partially. DØ and ANAPHE have been developed free of the constraints inherent in unplanned upgrades of existing equipment and their designs are a radical departure from the current detectors.

Both DØ and ANAPHE have a deep hermetic uranium calorimeter in order to obtain the best possible energy resolution on jets and ν 's. A hermetic calorimeter does not simply require full coverage in θ but also careful attention to cracks and dead regions in the calorimeter (which should not project to the origin) and also μ identification. None of the original detectors have such good calorimetry and none can achieve it by upgrading; the original hadron calorimeters with their abundance of projective cracks cannot be modified and their is insufficient space to introduce substantial additional hadron calorimetry.

The second key feature of the DØ and ANAPHE designs is the quantitative improvement in the identification of electrons and muons. In the case of electrons these detectors possess extremely fine-grained electromagnetic calorimeters (at least an order of magnitude finer than the original experiments) and an additional ability to reject hadrons, by means of transition radiation detectors. The combination of these features (especially with a magnetic field) will allow analysis of electrons at much smaller values of E_T and without the severe isolation requirements imposed in the current analyses of UA1 and UA2. The UA1 upgrade involves a first-class electromagnetic calorimeter of similar granularity but does not include a transition radiation detector. In the case of muons, the original detectors had inadequate absorber. Both DØ, ANAPHE and the upgraded UA1 have a minimum of $10\lambda_{\text{ABS}}$ absorber.

The differences between DØ and ANAPHE are less striking than with the first-generation detectors. The most important differences are that the ultimate version of ANAPHE can include a superconducting solenoid, whereas DØ cannot, and that ANAPHE proposes a new compact and precise central tracking system. The combination of these features will result in a detector of unmatched performance; it will allow competitive and distinct physics discoveries to continue at the Sp̄pS Collider even after TeV I and its detectors are fully operational.

We will now make an individual comparison of ANAPHE (with its superconducting solenoid) and each of the four hadron collider detectors. We have tabulated (Table 1) the important characteristics to facilitate this comparison. (Undoubtedly Table 1 will contain some errors because our sources of information are out-of-date. However, the spirit of this comparison is not to search for subtleties but to understand the basic differences in design and performance - and these should be correctly

4.2 Upgraded UA1

The upgraded UA1 calorimeter will provide a $2\lambda_{\text{ABS}}$ layer of uranium in front of the present coarse-grained $4.7\lambda_{\text{ABS}}$ Fe calorimeter. This will improve the jet and missing E_{\perp} performance somewhat but the uranium will only see a small part of the hadron shower and cannot provide effective compensation. The lack of hermeticity in the overall calorimeter will not be greatly improved - the most serious problems being the crack at the joint of the two halves of the magnet and cracks elsewhere in the calorimeter such as in the horizontal plane and at $\theta = 90^{\circ}$ and $\phi = \pm 45^{\circ}$. The ANAPHE uranium calorimeter is $6.3\lambda_{\text{ABS}}$ in depth and will provide a large improvement in the measurement of jets relative to a steel device (see e.g. Fig. 2 of SPSC/M376). The precision of measurement of jet mass and jet angle is further improved relative to UA1 by a substantial increase in hadron calorimeter granularity.

The central drift chamber of UA1 has excellent visual and tracking qualities. The main disadvantages are its slow speed (4 μ sec maximum drift time) and the lack of good momentum information for high p_{T} tracks emerging near to the horizontal plane i.e. parallel to the B field. A minimum projected track length of 40 cms is typically required and this gives a 30% track loss. In those analyses which require the combination of good central drift chamber information and good calorimetry, a substantial part of the azimuth must be excluded since the regions of poor measurement do not overlap. The ANAPHE detector and a solenoidal field has uniform azimuthal acceptance and momentum precision over the full central region $|\eta| < 1.5$.

In the case of electron identification, the quality of electromagnetic calorimetry is similar in both detectors but ANAPHE has $\sim 100 : 1$ extra πe rejection from transition radiation detectors. The detectors have similar performance for muon identification although the π/K decays, which dominate the background rate, are smaller in ANAPHE because there is one half of the decay path.

4.3 Upgraded UA2

The original design of the UA2 detector correctly anticipated the importance of calorimetry. However, the UA2 geometry is rather inflexible and a substantial upgrade is impossible. Although the new end caps lead to

a major improvement in the hermeticity of the detector there are still weaknesses associated with (a) cracks in the (totally projective) geometry of the calorimeter, (b) shallow central calorimeter depth, (c) shallow calorimetry at the interface of each end cap with the central ball and (d) the absence of muon identification. The upgrade does not substantially improve the performance or granularity of the central calorimeter - precisely the region where the most important physics occurs. A consequence of the relatively coarse calorimeter granularity is that electron analysis is restricted to isolated tracks, such as from $W \rightarrow e\nu$. If a scintillating fibre tracker and transition radiation detector are implemented there would be an improvement in πe rejection by a factor ~ 10 .

4.4 CDF

CDF places a strong emphasis on tracking and has a large volume drift chamber and good, uniform momentum measurement accuracy over the central rapidity region. The hadron calorimetry, although representing a bold step at the time of the proposal in 1981, is relatively poor in the light of current data: it has steel absorber, the granularity is coarse and there are many projective cracks between the calorimeter cells and at the connection of the magnet end plugs and the return yoke.

The electromagnetic calorimeter towers also have coarse granularity, although wire chambers embedded in these towers will improve the performance. There are no additional devices to improve the πe separation. In the case of muons, the CDF detector has the longest decay path and therefore highest π/K decay rate of any of the detectors. It also has an inadequate absorber thickness of only $6.5\lambda_{\text{ABS}}$.

CDF is unique in developing an extensive forward detector. Our approach is that instrumentation in the forward direction is necessary only for jet measurements and calorimeter hermeticity and that the emphasis on electron identification etc. should be made in the central region, which contains the hard scattering processes.

4.5 DØ

In its non-magnetic 1st phase, ANAPHE has essentially identical performance to DØ, but at about one half of the cost. The main

differences at this stage will be in the quality of the central tracking (e.g. ~ 120 hits per track vs. 24 for DØ and precision secondary vertex measurements in ANAPHE) and in the depth of transition radiation detectors (40cm vs. 25cm for DØ).

However, after adding a superconducting solenoid, ANAPHE will have a performance unmatched by any detector - a unique combination of high-quality calorimetry, momentum measurement, tracking and lepton identification. We have summarized the issues concerning the addition of a magnetic field in Table 2. The field will result in a substantial improvement in the overall performance of ANAPHE - especially for electron identification, where the sign will be measured and the detector will be able to handle electrons at much lower E_T and in the presence of jets because of the extra rejection afforded by E/p matching.

5. SUMMARY

We argue that the SppS Collider with ACOL has an excellent potential for exciting new physics but that the upgrades to the current detectors are an inadequate match to this physics. We have presented the conceptual design of a detector with unique performance which is not only superior to the upgraded UA1/UA2 detectors but also to the Fermilab TeV I detectors, CDF and DØ. We believe this detector would ensure the continuity and the competitive role of the SppS Collider even after the startup of TeV I. Furthermore, we consider this detector to be a powerful investment for the future of CERN, should the LHC develop. We are proposing a strategy which allows the detector to be built in the minimum time and with the minimum resources; the detector is phased and uses as much existing equipment and infrastructure as possible. The project will require a larger effort than available within our current collaboration and we urge the SPSC to recommend that a work study group - drawn from members of all UA collaborations, ourselves and other interested physicists - be organised forthwith to develop a second generation calorimeter detector for the SppS Collider with ACOL.

6. ACKNOWLEDGEMENTS

We wish to thank members of the UA2 collaboration for help with ISAJET Monte-Carlo programs.

APPENDIX A

TEST RESULTS OF A TOWER STRUCTURED SCINTILLATOR-LEAD PHOTON CALORIMETER
USING A NOVEL FIBER OPTICS READOUT SYSTEM

In this section we describe briefly the test results which we obtained with a tower structured scintillator-lead photon calorimeter using a novel fiber optics readout system. More details can be found in ref. [1].

The test calorimeter is divided into 9 individual towers. Each tower has a cross-section of $5 \times 5 \text{ cm}^2$ and consists of 60 layers of 2 mm lead plus 5 mm thick scintillator (KSTI 390)(Fig. 6). The four sides of each tower are covered by thin acrylic sheets (1.5 mm thick) doped with wavelength shifting (W.S.) material (Coumarin 250 mg/l). The light produced in each scintillator plate is first converted in these sheets, then converted a second time in a set of polysterene optical fibers (ϕ 2 mm and 11 m attenuation length) doped with K-27 w.s. material (200 mg/l) which were longitudinally through the calorimeter along the corners of each tower. A small diameter photomultiplier (Hamamatsu R647-1) was attached to the fibers at the back end of the calorimeter.

The test was performed in a test beam (T10) of the PS at CERN. We investigated the energy resolution and the uniformity of response. The calorimeter was exposed to incident electrons with energies of 250 MeV, 500 MeV, 1 GeV, 2 GeV, 3 GeV and 5 GeV.

The energy resolution of the calorimeter was measured with the electron beam hitting the central tower of the calorimeter. The obtained energy resolution as a function of $1/\sqrt{E}$ is shown in Fig. 7. A linear fit through the data points gives:

$$\sigma/E = 0.01 + \frac{0.10}{\sqrt{E}} \quad (1)$$

The energy resolution due to sampling fluctuation

Monte-Carlo simulation program (EGS-code). The energy resolution was calculated using a

$$(\sigma/E)_s = 0.075/\sqrt{E}$$

(2)

From this, the energy resolution $(\sigma/E)_{Ne}$ due to photoelectron statistics, with Ne the number of photoelectrons per GeV deposited energy, can be estimated using the relation:

$$\left(\frac{\sigma}{E}\right)^2 = \left(\frac{\sigma}{E_s}\right)^2 + \left(\frac{\sigma}{E_{Ne}}\right)^2 \quad (3)$$

one obtains

$$\frac{\sigma}{E}_{Ne} = \frac{.066}{\sqrt{E}} \quad (4)$$

Comparing (2) and (4) the energy resolution of the calorimeter results in equal parts from the resolution due to sampling fluctuations and photoelectron statistics. The obtained photoelectron yield per minimum ionizing particle per layer is 1.3.

The uniformity of response of the calorimeter was studied with 5 GeV electrons performing a horizontal scan through the towers with the number 5,8,6 and a diagonal scan through the towers 1 and 2 as indicated in Figs. 8(a,b) respectively. For this uniformity scan the electron axis was parallel to the w.s. sheets and the fibers. The results show a $\pm 2\%$ non-uniformity for the horizontal scan and a comparatively large non-uniformity for the diagonal scan probably due to Cerenkov light produced in the fibers and (or) direct scintillator light reaching the fiber. The uniformity at the corners of the towers can possibly be improved in the future by preventing the direct scintillator light to reach the fibers (black paper covering the calorimeter corners) and by choosing a non-projective tower geometry.

The introduction of optical fibers for reading out calorimeter towers offers the following advantages:

- (1) The small diameter flexible fibers allow the transmission of the scintillator light from the calorimeter towers over many meters to the photomultipliers with low loss. This is an important characteristic

- (2) The light of a tower with any size or shape can be collected onto a small diameter photomultiplier or a small area silicon photo-diode.
- (3) A simple and compact construction with minimal dead space between individual cells is possible, and complicated and expensive structures of conventional light guides are avoided.

In a previous publication Ref. [2], we have demonstrated that the double wavelength shifting technique offers also the possibility to readout small size individual scintillator towers which are sandwiched with large size converter plates. Only small holes in the converter material are needed to let the optical readout fibers pass through. With this technique the dead space of the converter material can be minimized.

Encouraged by these results we are presently performing further tests to improve the light collection efficiency, the uniformity and to study the use of silicon photodiodes instead of photomultipliers. The main advantages of silicon photodiodes as compared to photomultipliers are their stability, their insensitivity to a magnetic field, their small size and their relatively low price.

REFERENCES

- [1] H. Fessler et al., MPI-PAE/Exp. ER. 132, (June 1984), to be published in Nucl. Inst. & Meth.
- [2] J. Fent et al., Nucl. Instr. & Meth. 211 (1983) 315.

TABLE 1: PERFORMANCE COMPARISON OF $\bar{p}p$ DETECTORS

Item	UA1 (u/g)	UA2 (u/g)	CDF	D ϕ	ANAPHE
<u>1. HADRON CALORIMETRY (central region)</u>					
1.1 Type : Absorber Readout	U + Fe Sc/double WS	Fe Sc/WS	Fe Sc/WS	U/Cu LAR	U/Cu Sc/double WS
1.2 Perpendicular thickness inc.em.cal. (λ_{ABS})	1.8(U)+4.7(Fe)	4.4	6.5	6.9	6.3
1.3 Sampling thickness (X_0)	.6+2.8	.9	1.4	.5+1.3	.5+1.0
1.4 Number of towers	1200+128	240	380	580	1450
1.5 Approximate cell size ($\Delta\phi\Delta\eta$, $\theta=90^\circ$)	.13x.13+.39x.26	.26x.17	.26x.11	.15x.17	.12x.12
1.6 σ_E/E (%)	40/√E?	60/√E?	62/√E	36/√E	36/√E
1.7 e/π relative response	1.1?	1.4	1.4	1.1	1.1
1.8 $\sigma_{\Sigma E_t} / \Sigma E_t$.3/√ΣE _t ?	.5/√ΣE _t	.5/√ΣE _t	.3/√ΣE _t	.3/√ΣE _t
1.9 Hermeticity comments	Fe calorimetry has projective geometry with wavebar cracks Δφ=±10° region in vertical plane affected by magnet gap	Projective geometry with wavebar cracks	Projective geometry with wavebar cracks Dead gaps at end plug interface	Cryogenic gaps (non-projective)	Readout fibre holes (non-projective)
		Shallow calorimeter depth			
		Thin calorimetry between barrel and end-cap			
		No μ identification			

TABLE 1 (Cont'd): PERFORMANCE COMPARISON OF PP DETECTORS

Item	UA1(u/g)	UA2(u/g)	GDF	DØ	ANAPHE
2. ELECTROMAGNETIC CALORIMETRY (central region)					
2.1 Type: Absorber Readout	U Sc/double WS	Pb Sc/WS	Pb Sc/WS	U/Cu LAR	U/Cu Sc/double WS
2.2 Inner radius (cms)	120	60	165	70	60
2.3 Perpendicular thickness (X_0)	24	17	20	24	35
2.4 Sampling thickness (X_0)	.6	.6	.6	.5	.5
2.5 Depth segmentation (X_0)	3/6/9/6	17	20	2/2/6/14	4/27/4
2.6 Number of towers	1200	240	480	3400	5800
2.7 Approximate cell size ($\Delta\phi\Delta\eta, \theta=90^\circ$)	.13x.13	.26x.17	.26x.11	.075x.075	.06x.06
2.8 σ_E/E (%)	10/VE	14/VE	14/VE	10/VE	10/VE
2.9 Calibration systematics (%)	2	2	2	.1	2
2.10 Comments	1 em section, cell size =.07x.07	1.5 X_0 W pre-shower counter	Wire ch. at 3&6 X_0		Can be up- graded to .03x.03 cell size.
3. MAGNET/TRACKING					
3.1 Magnet type	Horizontal field dipole	-	Sc solenoid	-	[Sc solenoid](*)
3.2 B field (T)	0.7	-	1.5	-	[1.5]
3.3 Tracking type	Long-drift (20cm) DC	MWPC+ jet ch.	Jet ch.	Jet ch.	Scintillating optical fibres
3.4 Number of hits per track	110	18	60?	24	120
3.5 Measurement precision per hit (μm)	100+350	200 (jet ch.)	200	200	10
3.6 Two-track resolution (mm)	3-5	3	3	3	.05
3.7 σ_p/p	.5%p	-	.3%p	-	[.04%p @4%](**)

(*) {} implies after sc solenoid upgrade.
(**) @ implies addition in quadrature.

TABLE 1 (Cont'd): PERFORMANCE COMPARISON OF \bar{p} DETECTORS

Item	UA1(ν/g)	UA2(ν/g)	CDF	D ϕ	ANAPHE
<u>4. LEPTON IDENTIFICATION</u>					
4.1 Neutrinos (see items 1.6-1.9)					
<u>4.2 Electrons</u>					
a) Sign measurement	yes	no	yes	no	[yes] (*)
b) Calorimetry (see item 2)					
c) Additional hadron rejection	-	TRD (15cm depth)	-	TRD (25cm depth)	TRD (40cm depth)
<u>4.3 Muons</u>					
a) Absorber thickness @ $\theta=90^\circ$ (λ_{ABS})	9	-	6.5	13	10
b) Decay path length @ $\theta=90^\circ$ (cm)	140	-	195	90	80
c) Number of independent momentum measurements	3	-	1	1	1 [3]

TABLE 2

The Influence of a Central Magnetic Field on a Calorimeter Detector

Advantages

1. Measurement of e sign
2. Improvement in e identification:
 - p/E match
 - e⁺e⁻ pairs separated
3. Improvement in μ identification and measurement (by matching Pinner and Pouter e.g. in Fe toroids):
 - reduce punch-throughs
 - reduce $\pi/K + \mu$ decays
 - correct determination of μ direction cosines at origin
 - rejection of μ 's with bad momentum measurement.
4. Measurement of momentum/sign of all tracks:
 - invariant masses e.g. heavy flavour tag from D*, B reconstruction
 - lifetime measurements
5. Independent jet measurements
 - P_T filter
 - precise measurement of jet angles using stiff tracks
6. Extra redundancy for isolating rare signals
7. Internal cross-check of calorimeter energy measurements.

Disadvantages

1. Cannot identify e⁺e⁻ pairs by dE/dx. (The two methods - dE/dx or tracking of pairs - are probably equally effective in well-designed experiments.)
2. Tracking is harder and requires more radial space (for conventional trackers).
3. Extra Cost

FIGURE CAPTIONS

- Fig. 1 Electron spectrum from $b \rightarrow ce\nu$ decays according to ISAJET $b\bar{b}$ jets produced in the range $20 < E_t^b < 35$ GeV.
- Fig. 2 Rapidity distribution of b primary electrons produced in the decays $W \rightarrow t\bar{b} \rightarrow Xb\bar{b}$ followed by $b/\bar{b} \rightarrow c/\bar{c} e\nu$.
- Fig. 3 $d\sigma/dp_T$ distributions which are relevant in a search for prompt electrons from $W \rightarrow t\bar{b}$. We show d) the single charged particle cross-section and a) the signal rates from $t \rightarrow be\nu$ and $b \rightarrow ce\nu$ decays. Also indicated are the raw rates, before any further cuts, for overlap of a π^\pm and γ in the same electromagnetic calorimeter cell according to c) non-magnetic and b) magnetic ANAPHE. In both cases p_T^γ is plotted and p_T^π is c) unrestricted and b) required to equal p_T^γ within ± 1 GeV/c.
- Fig. 4 $d\sigma/dp_T^{\text{missing}}$ distributions according to ISAJET events with a requirement of at least one jet having $p_T > 20$ GeV/c. The curves show:
- Gluino pair production and decay to $g\tilde{\gamma}$ ($m_g^\nu = 70$ GeV/c²).
 - The "perfect detector" rate where all particles, except ν 's are perfectly identified and measured. The ν 's are produced both by heavy flavour decay and by π/K decay-in-flight, prior to the calorimeter.
 - The ANAPHE detector with uranium end caps.
 - The ANAPHE detector with UA2 upgrade end caps.
 - The upgraded UA2 detector.

The calorimeters are assumed to have no cracks and their coverage extends to an angle of 5° with respect to the beam axis..

Fig. 5 $d\sigma/dp_T^{\text{missing}}$ distributions according to ISAJET events with a requirement of at least one jet having $p_T > 20$ GeV/c. The curves show:

a-c) As Fig. 4.

d) The ANAPHE detector with uranium end caps and 8 azimuthally projective cracks in the calorimeter totalling $5\% \times 2\pi$ radians. The cracks are massive (i.e. filled with inert material) and incident particles are assumed to have a mean response of $1/2$ relative to nominal.

e) As in d) but with massless cracks. Incident particles exit the calorimeter without depositing any energy.

Fig. 6 Configuration of the scintillator lead photon calorimeter. The double wavelength shifter readout using optical fibers for one tower is shown in detail.

Fig. 7 The energy resolution σ/E for incident electrons with 250 MeV, 500 MeV, 1 GeV, 2 GeV, 3 GeV and 5 GeV are shown. The straight line represent a linear fit through the data points.

Fig. 8(a) The peak pulse heights obtained from a horizontal scan over towers 5, 8 and 6. The summed signals of all PM's (1-9) are shown by open circles. The signals of the individual PM's 5,8,6 are shown as crosses.

(b) The peak pulse heights obtained from a diagonal scan over towers 1 and 2. The open circles show the sum of the signals from all PM's (1-9), the crosses (+, x) the signals from PM1 and PM2 respectively, and the dots, the sum of signals from PM3 and PM4.

ELECTRON SPECTRUM

b jets P_T 20-35 GeV/c
↳ c e ν

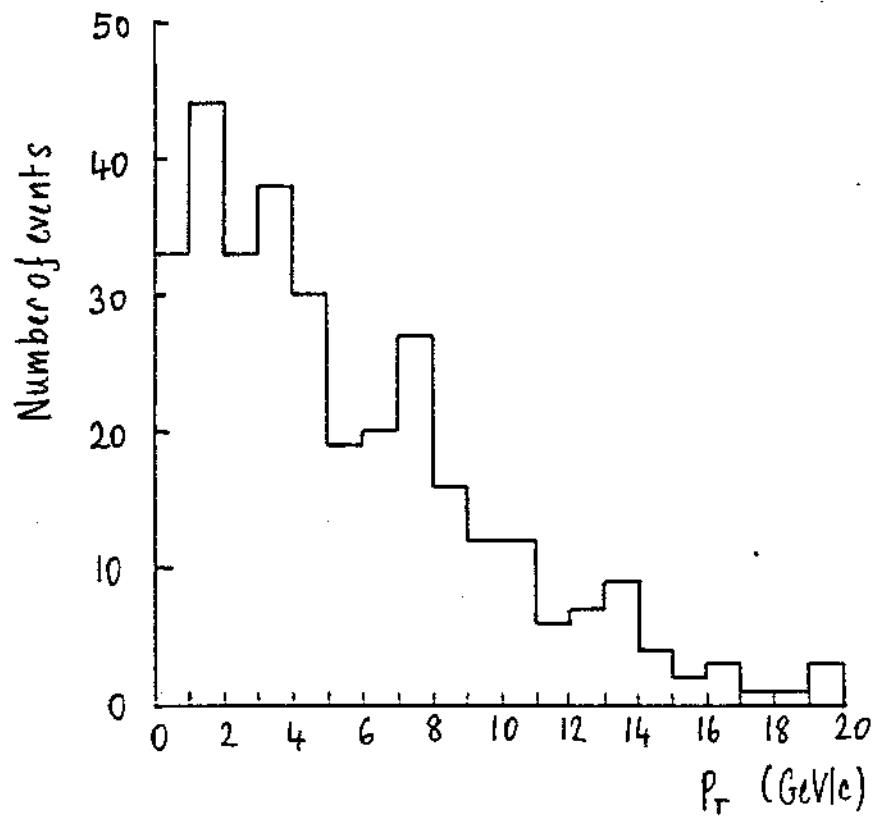
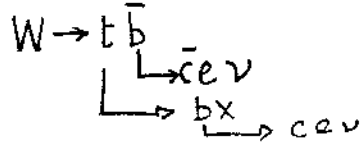


FIG 1

ELECTRON PSEUDORAPIDITY



[ARROWS MARK LIMITS OF CENTRAL U
CALORIMETER + TRDS]

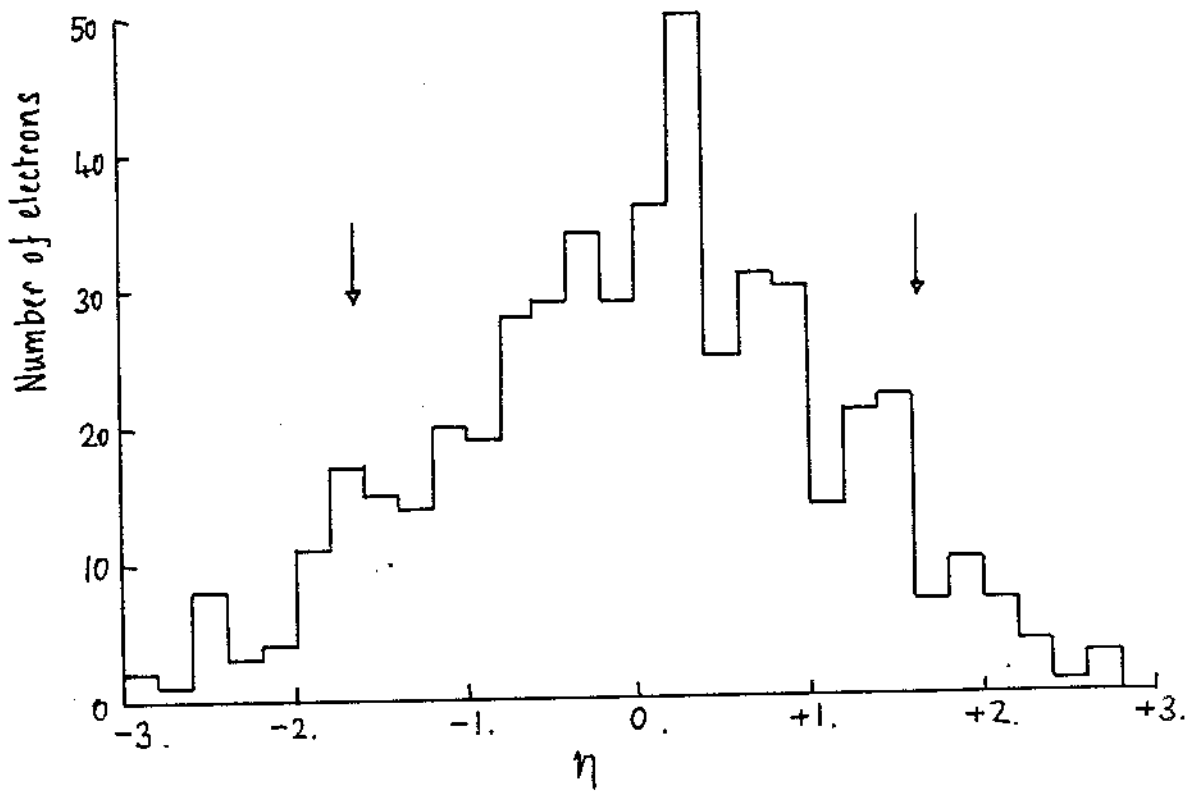


FIG 2

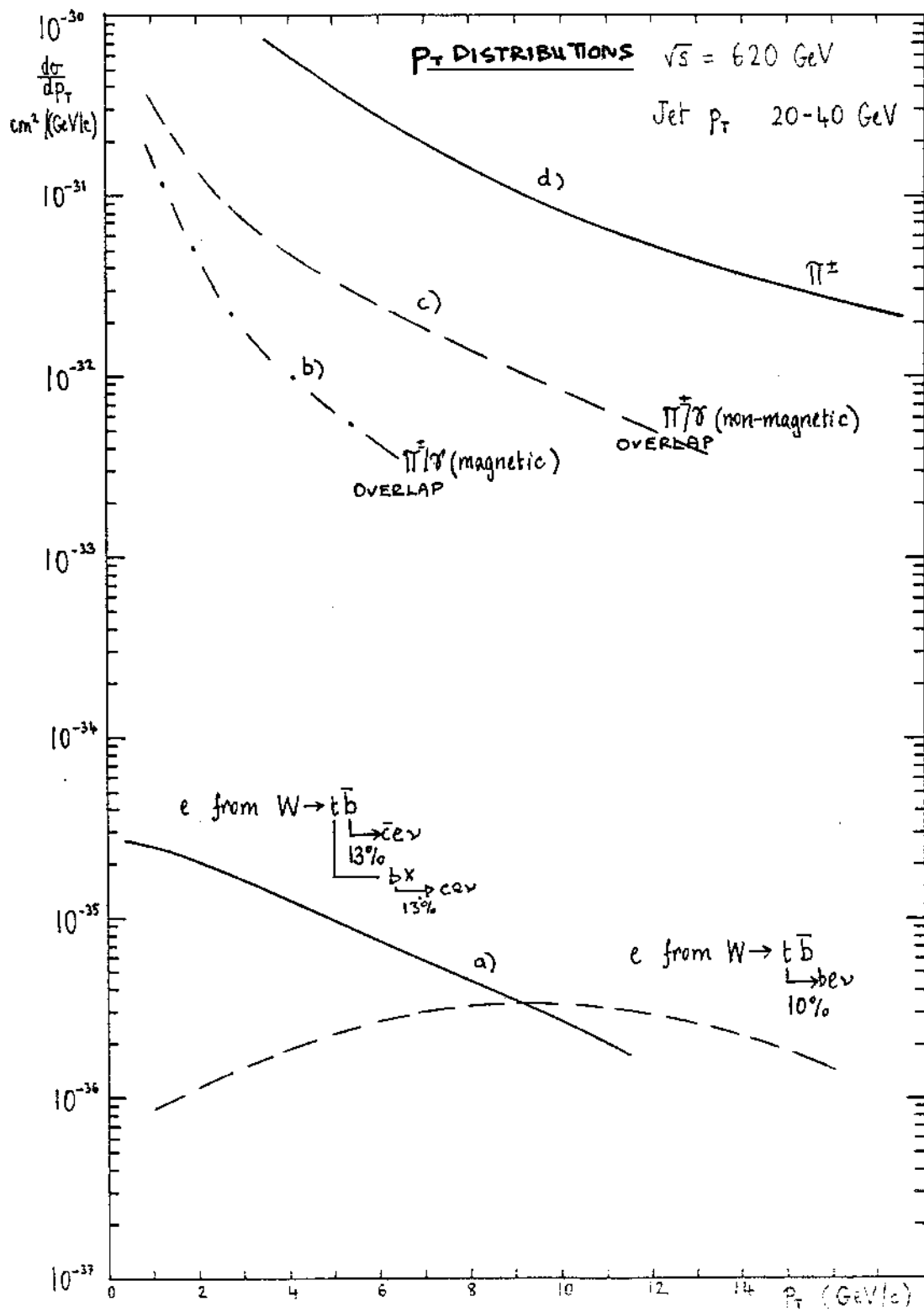


FIG 3

MISSING p_T

$\sqrt{s} = 620 \text{ GeV}$

Jets p_T 20-40 GeV/c

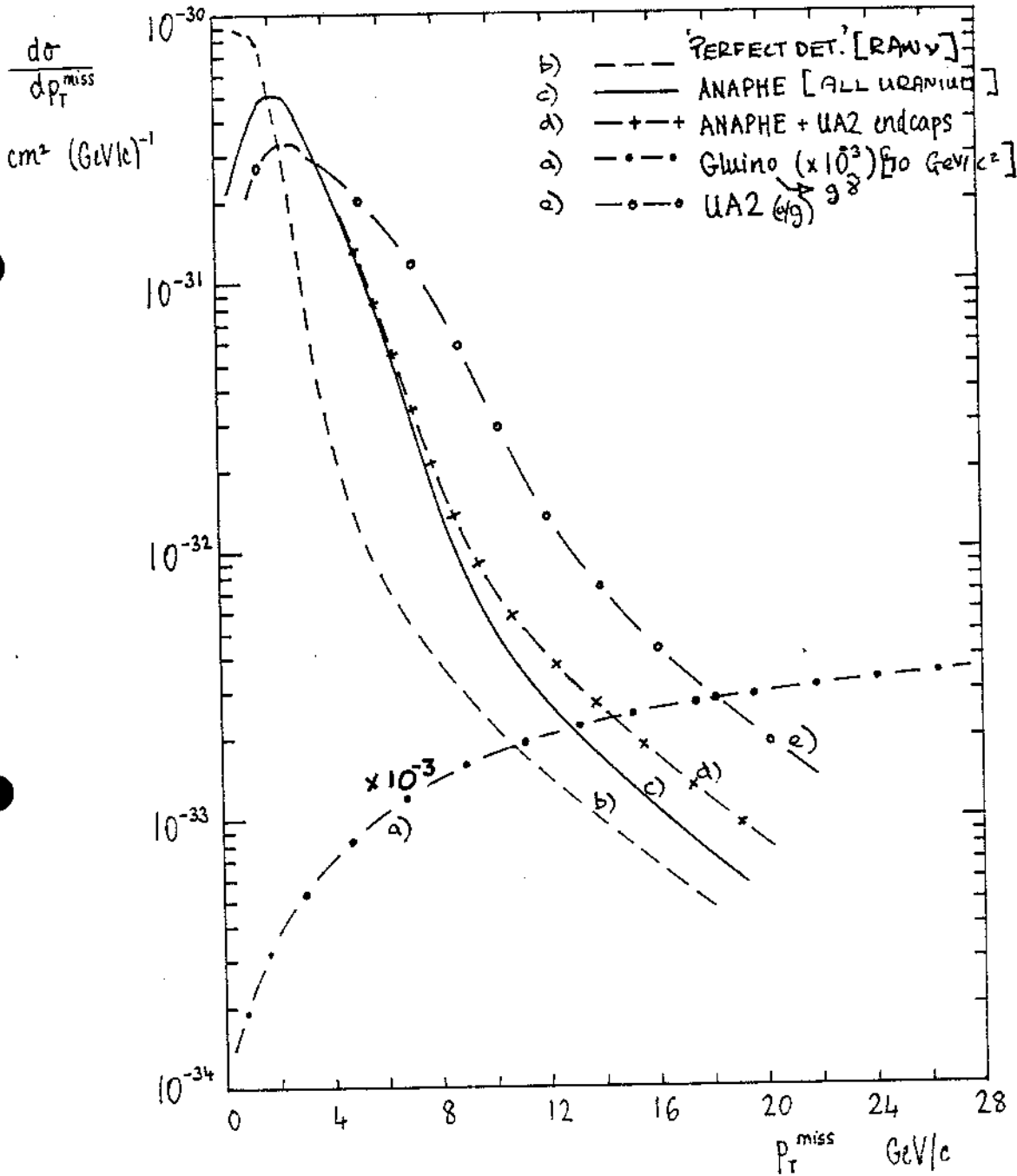


FIG 4

MISSING P_T $\sqrt{s} = 620 \text{ GeV}$
 Jets P_T 20-40 GeV/c

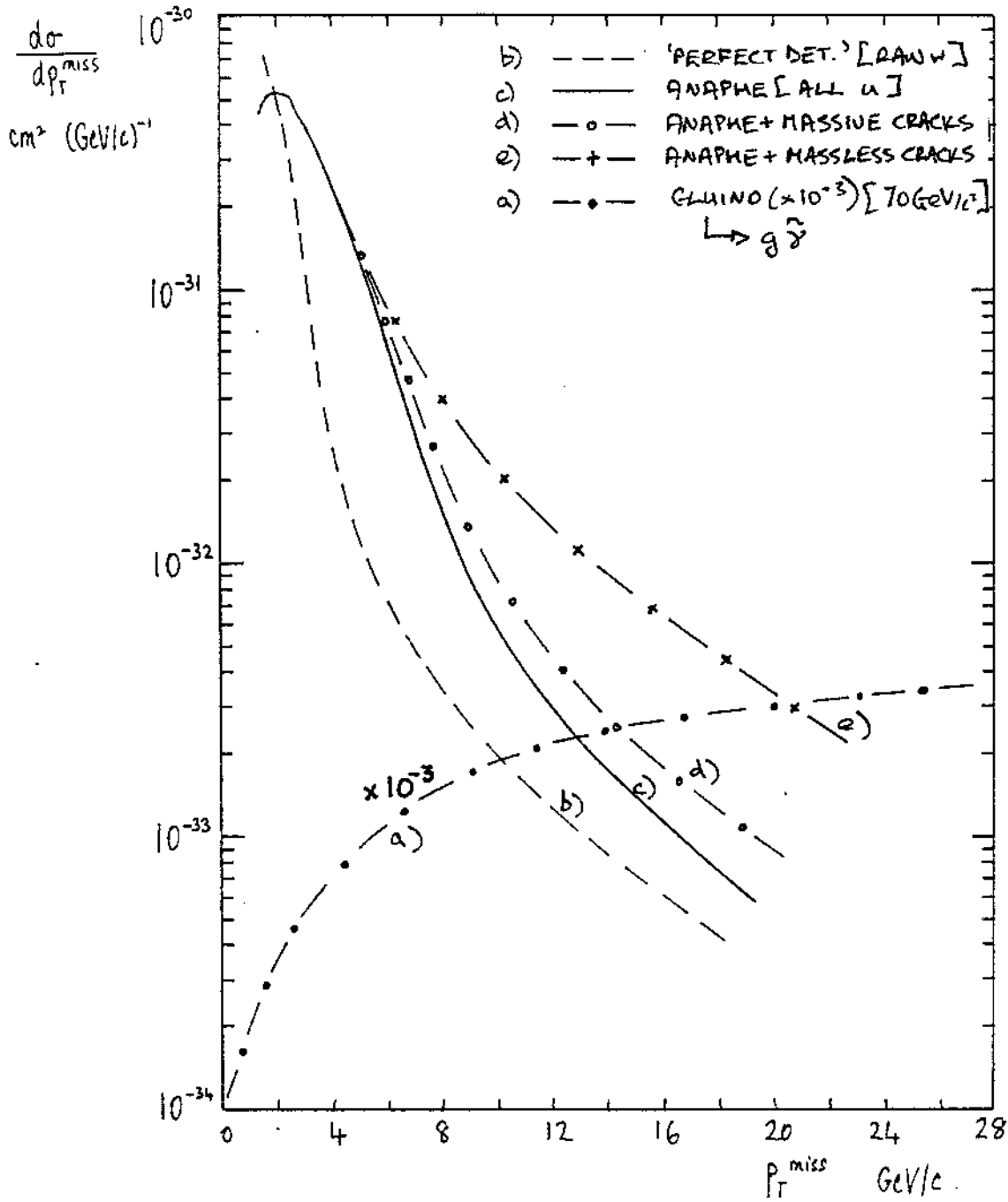


FIG 5

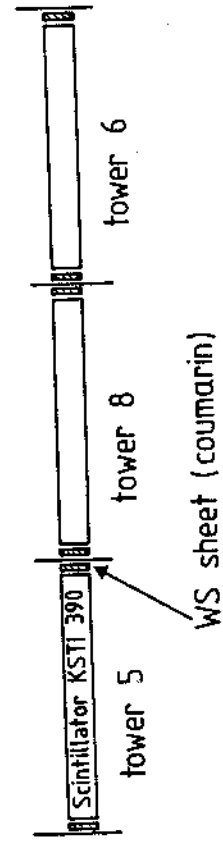
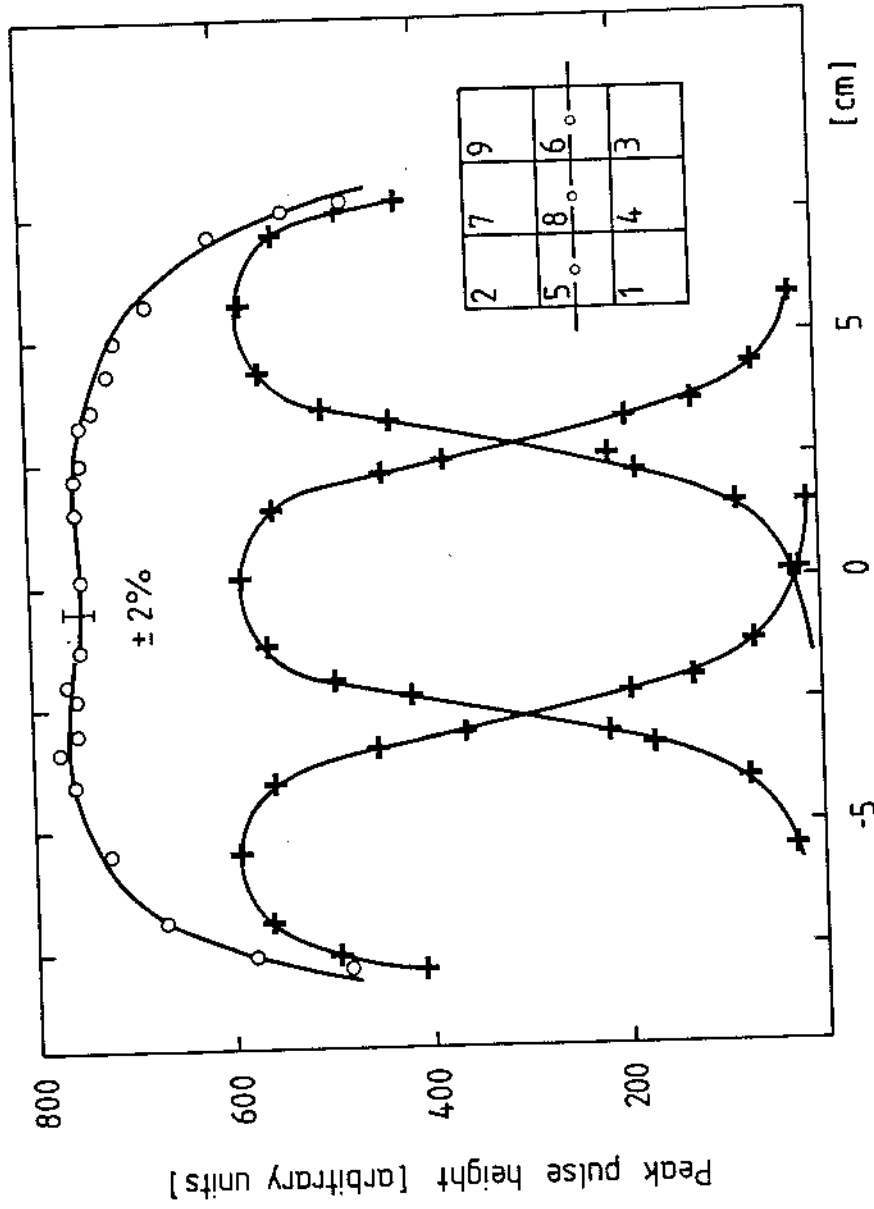


Fig 8a)

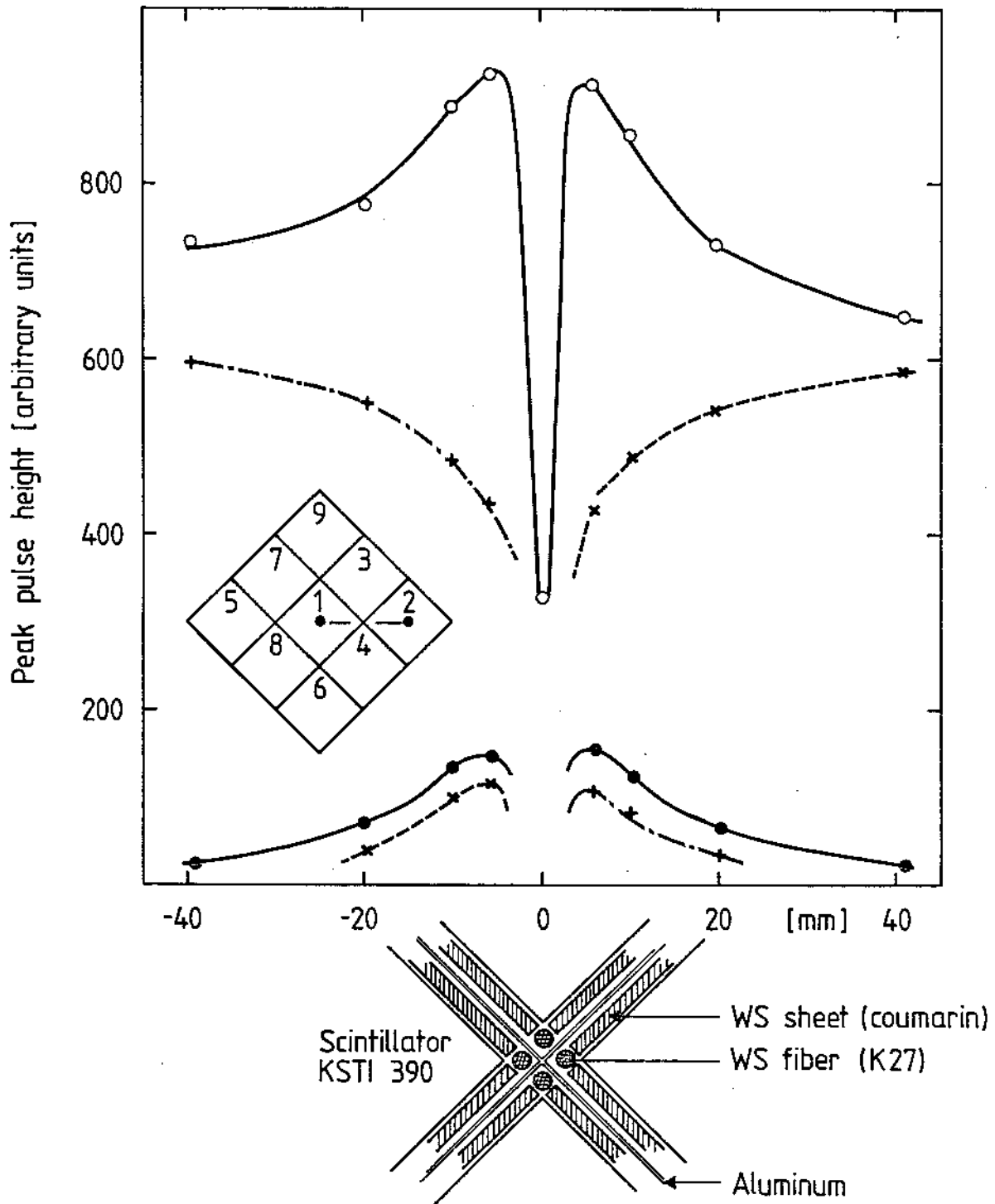


Fig 86)

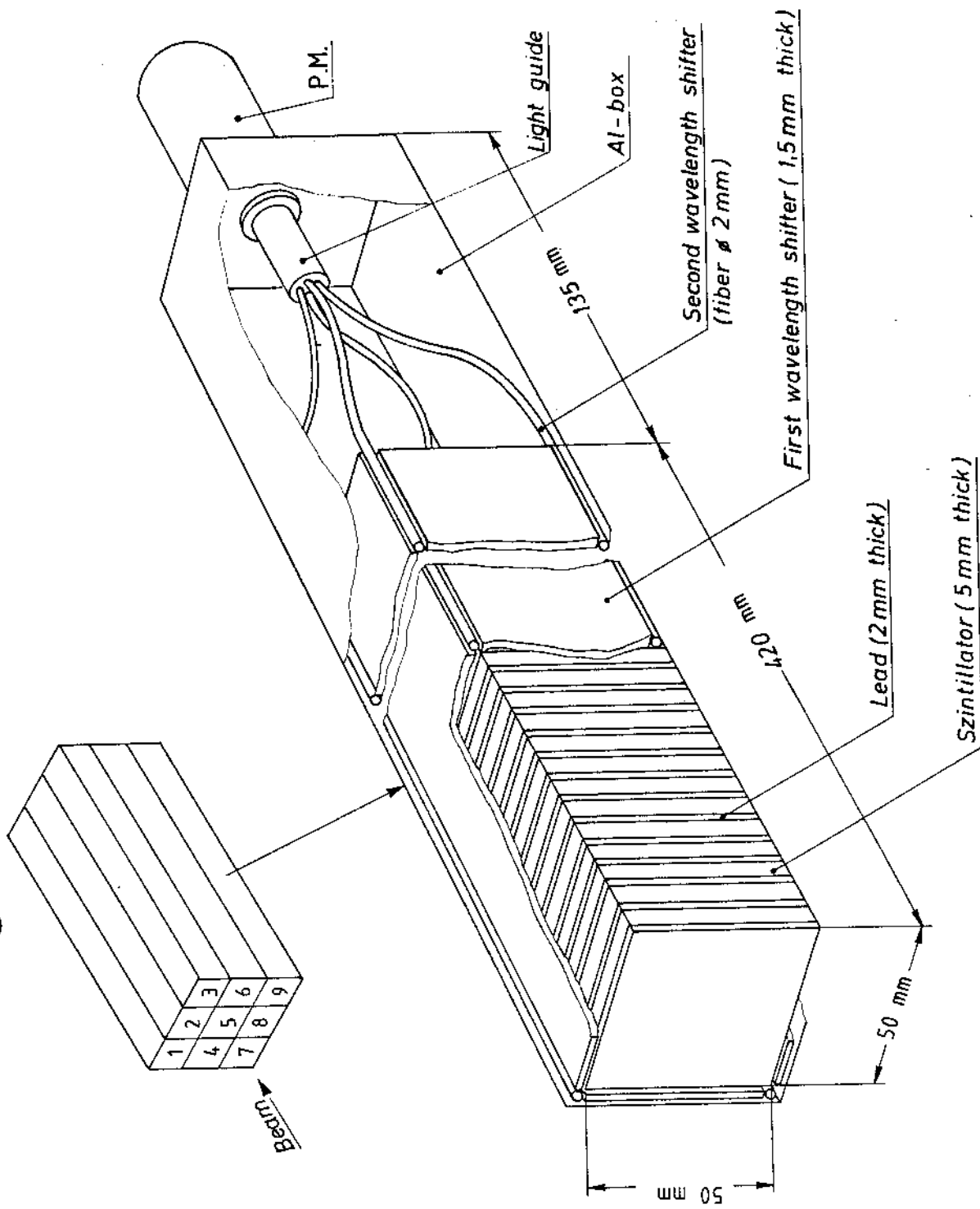


Fig 6

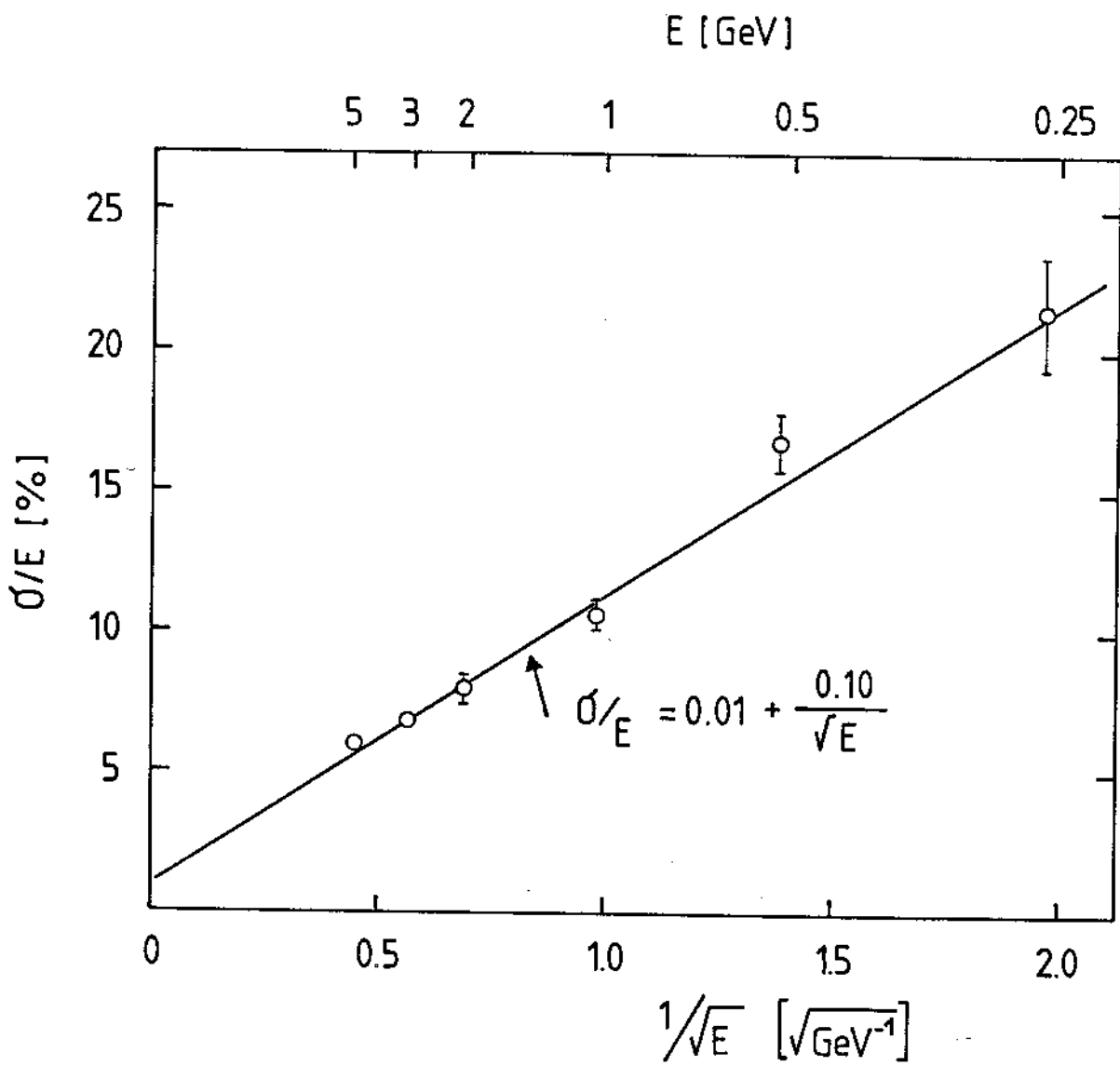


Fig 7